Self-propelled Leidenfrost drops on a thermal gradient: A theoretical study

B. Sobac,[1,a)] A. Rednikov,[1] S. Dorbolo,[2] and P. Colinet[1]
[1]*TIPs-Fluid Physics, Université libre de Bruxelles, Brussels, Belgium*
[2]*CESAM-GRASP, Physics Department, Université de Liège, Liège, Belgium*

(Received 1 March 2017; accepted 16 June 2017; published online 2 August 2017)

We theoretically investigate the behavior of Leidenfrost drops on a flat substrate submitted to a horizontal thermal gradient and highlight that they are able to self-propel in a preferential direction. Namely, they are found to travel towards the colder parts of the substrate, as if they were trying to maximize their lifetime. In particular, a centimetric water drop can reach velocities of the order of cm/s for thermal gradients of the order of a few K/mm. In general, the presented model, based upon the lubrication approximation in the vapor cushion as in the work of Sobac *et al.* ["Leidenfrost effect: Accurate drop shape modeling and new scaling laws," Phys. Rev. E **90**, 053011 (2014)] and here formulated for simplicity for a 2D drop, enables predicting the values of these velocities as a function of the thermal gradient, drop size, superheat, and fluid properties. Surprisingly, the variability of vapor properties with temperature turns out to be instrumental for the drop to move, even if the vapor film profile is always asymmetric anyway. Finally, this asymmetry being typically weak, its effect also proved to be well captured by linearization around the corresponding symmetric Leidenfrost state. *Published by AIP Publishing.* [http://dx.doi.org/10.1063/1.4990840]

I. INTRODUCTION

When a liquid drop is deposited over a solid surface whose temperature is sufficiently above the boiling point of the liquid, the drop does not experience nucleate boiling but rather quietly levitates over a thin layer of its own vapor (Leidenfrost effect[1]). The absence of contact with the surface considerably reduces the friction and confers an extreme mobility to the drop.

Linke *et al.*[2] found that, when placed on an asymmetrically textured surface (such as ratchets), Leidenfrost drops can self-propel in a preferential direction with a velocity of the order of tens cm/s. The physics and the hydrodynamics leading to the propulsion of such drops have been extensively investigated.[3–11] Various mechanisms have been suggested and the main mechanism responsible for the force acting on the drop has been under debate. However, recently, several studies presented evidence in favor of the "viscous mechanism" as the main driver of the motion.[3,8,9] The idea is that the vapor flow below the levitated drop is rectified by the asymmetric teeth of the ratchet. The vapor flows in a preferential direction, along the descending slope of each tooth. As a consequence, the resulting viscous stress entrains the drop in the same direction.

These findings open new doors to the control and manipulation of drops. This can indeed be particularly useful in systems where drops need to be transported rapidly and accurately. Playing on the geometry of the texture, it is then possible to control the velocities and trajectories of Leidenfrost drops and even to immobilize them.[5,7,11,13] Another control approach using a magnetic field on a paramagnetic Leidenfrost drop has also been explored.[14]

The motion of a number of different objects in the Leidenfrost state has been investigated up until now, as reported in Fig. 1. The levitating object can be a liquid drop which self-propels when placed on a ratchet-like surface[2] [see Fig. 1(a)]. It can also be a platelet of solid carbon dioxide, also called dry ice, self-propelling when placed on a ratchet-like surface[12] [see Fig. 1(b)]. With a sublimation point at −78 °C, the solid directly generates vapor and levitates in the Leidenfrost state. Finally, the behavior of uneven pieces of dry ice on a horizontal smooth plate has been studied[12] [see Fig. 1(c)]. Adding a small weight on one side of the platelets, an asymmetry of the solid mass distribution is created, leading to a tilted solid and a non-uniform thickness of the vapor layer. The vapor layer being thinner where the solid is heavier, the platelet self-propels in the direction of the added weight. In all these systems, it is worth noticing that an angle between the levitating object and the substrate is somehow present, which leads to propulsion. However, as remarked by Dupeux *et al.*,[12] the motion is directed toward the direction of closing angles for the asymmetric solid [see Fig. 1(c)], whereas it takes place in the direction of opening angles over a ratchet [see Figs. 1(a) and 1(b)].

Hence, the presence of a ratchet might not be the only way of generating self-propulsion of Leidenfrost drops. If an asymmetry of the vapor flow is sufficient, it might also be possible to make a Leidenfrost drop self-propel by generating a thermal gradient along a flat horizontal substrate. Indeed, the evaporation flux profile being asymmetric due to the substrate temperature non-uniformity, the bottom of the drop must become asymmetric as well, as if tilted by a small angle, with

a)Electronic mail: bsobac@ulb.ac.be

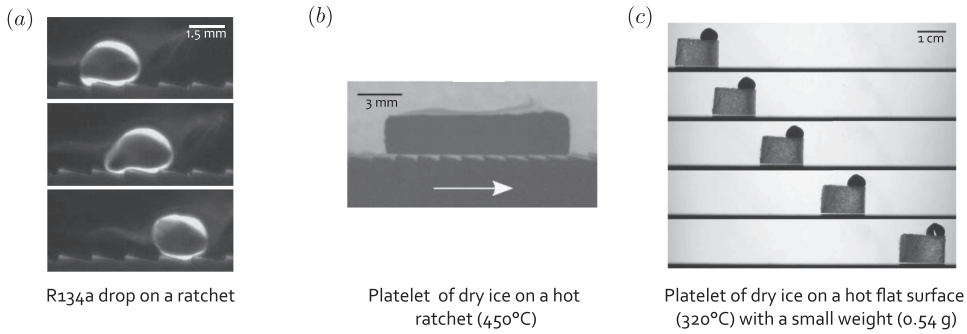

FIG. 1. The different configurations investigated up until now leading to self-propulsion of an object in the Leidenfrost state on a horizontal substrate. (a) Liquid drop on a millimetric ratchet-like topology surface. The image is reproduced with permission from Linke *et al.*, "Self-propelled Leidenfrost droplets," Phys. Rev. Lett. **96**(15), 154502 (2006). Copyright 2006 American Physical Society. (b) Dry ice platelet on a hot ratchet. (c) Dry ice platelet on a hot flat surface with a small asymmetric weight. The images [(b) and (c)] are reproduced with permission from Dupeux *et al.*, "Self-propelling uneven Leidenfrost solids," Phys. Fluids **25**, 051704 (2013). Copyright 2013 AIP Publishing LLC. In all these cases, a certain tilt between the levitating object and the substrate is involved, either continuous (asymmetric platelet) or piecewise (ratchet), which leads to propulsion.

the vapor film being thinner where the substrate is colder.[15] As a consequence, the drop should not remain at rest. By analogy with Fig. 1(c), it may rather be expected to self-propel in the direction opposite to the thermal gradient, i.e., in the direction of the closing angle. It is a theoretical study of this situation that forms the subject of the present paper. One of the goals is evaluating drop velocities that can be reached for reasonable values of the applied substrate temperature gradient. The paper is organized as follows: the model is developed in Sec. II, the results are presented in Sec. III, and the conclusions are summarized in Sec. IV.

II. FORMULATION DEVELOPMENT AND SOLUTION METHOD

Let us consider for simplicity a two-dimensional (planar) drop levitating above a hot substrate whose average surface temperature $\overline{T}_w$ underneath the drop is higher than the Leidenfrost temperature T_L (see Fig. 2). The size of the drop is measured by its maximum radius $R_{\max}$ (half of the size as seen from above), while the vapor film thickness profile is denoted as $h = h(x)$. The substrate is subject to a constant temperature gradient $\nabla T_w \equiv \vec{A}_w$. Thus, the substrate temperature $T_w = T_w(x)$ linearly depends on x, namely, $T_w(x) = \overline{T}_w + A_w x$, where $x = 0$ corresponds to the middle of the drop. The substrate temperatures at the left and right ends of the drop are denoted as $T_w^l = T_w(-R_{\max})$ and $T_w^r = T_w(R_{\max})$, respectively.

The present model is aimed at predicting the quasi-steady state of such a drop, including both its geometry and its possible translation as a whole. Indeed, the evaporation of Leidenfrost drops is typically long compared to thermal and viscous relaxation times, justifying our look for quasi-steady shapes only. The drop geometry is modeled by numerically matching the static equilibrium shape (for the upper part) with the lubrication solution for the vapor film underlying the drop (for the bottom part) as in Ref. 15. The translational drop motion is accounted for by considering the horizontal balance of forces acting on the drop bottom surface. As a first approach, quasi-steadiness is also assumed as far as the drop motion is concerned.

A. Upper part of the drop

The upper part of the drop surface is assumed to be governed by a balance between the hydrostatic and capillary pressures, i.e., just as for the static equilibrium shape of a superhydrophobic sessile drop. This simply reads

$$\sigma\kappa + \rho_\ell g(z - z_{\text{top}}) = \sigma\kappa_{\text{top}}, \tag{1}$$

where ρ_ℓ is the liquid density, σ is the surface tension, and g is the gravitational acceleration. Here, κ is the curvature of

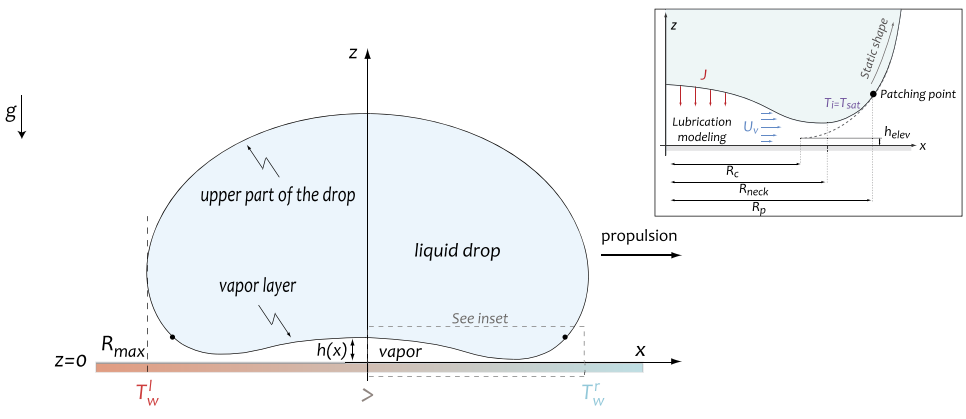

FIG. 2. Configuration studied. A liquid drop is deposited on a hot flat solid substrate submitted to a thermal gradient, due to which an asymmetry is created leading to the self-propulsion of the drop.

the drop surface (a function of the drop shape and its derivatives), while κ_{top} (curvature at the top of the drop, $z = z_{\text{top}}$) is a free parameter controlling the drop size. For a given value of the top curvature κ_{top}, numerically integrating this differential equation yields the corresponding equilibrium shape and value of $R_{\max}$. Inversely, for a given value of $R_{\max}$, we can thereby unambiguously obtain the corresponding shape and the value of κ_{top}. Note that it is in terms of $R_{\max}$ that the results will eventually be presented.

The solution of Eq. (1) also yields the height of the corresponding superhydrophobic sessile drop $H = H(R_{\max})$, hence $z_{\text{top}} = H$ for $z = 0$ is hereafter fixed at the substrate surface. For a Leidenfrost drop, however, the upper part shape coincides with the superhydrophobic drop only up to an additional vertical shift h_{elev}, accounting for the presence of a vapor layer underneath the drop (see the inset in Fig. 2), hence

$$z_{\text{top}} = H + h_{\text{elev}} \tag{2}$$

(instead of $z_{\text{top}} = H$). The vertical shift parameter h_{elev} is the only one of the upper part shape that remains undetermined at this stage for each given $R_{\max}$ within our approach.

Following Ref. 15, the upper part solution is assumed to be valid up to the patching points $x = \pm R_p$ (see Fig. 2) located at the outer edge of the vapor layer, somewhere between $R_{\max}$ and the contact radius of the corresponding superhydrophobic drop R_c. Between these points, in the vapor film, non-equilibrium effects of evaporation and viscous pressure losses in the vapor flow are important and affect the shape. However, in view of the asymmetry introduced by the temperature gradient, asymmetric patching points, $x = -R_p^l$ and $x = R_p^r$, will rather be used at the left and at the right as described in Sec. II B. Note that within the developed approach, any possible asymmetry becomes apparent through the vapor layer and the patching points, whereas the upper part shape, where any dynamic influence is neglected, naturally remains symmetric.

B. Vapor layer

The thickness of the vapor film $h(x)$ and its slopes are assumed to be small enough so that the lubrication approximation is applicable (in particular, $h \ll R_{\max}$ and $\partial_x h \ll 1$). The gas itself is there assumed to be composed of pure vapor (the air being supposedly washed out by the vapor flow). Then disregarding possible motions inside the drop, which is a feature of all similar models developed thus far[15–17] (partly justified by large dynamic viscosity ratios between the drop and the vapor), the pressure in the vapor film is found from the pressure jump at the interface as

$$P_v = P_0 - \rho_\ell g(h - h_{\text{elev}}) - \sigma\kappa, \tag{3}$$

where $P_0 = \sigma\kappa_{\text{top}} + \rho_\ell g H$ is the pressure at the bottom of the corresponding superhydrophobic drop (see Sec. II A). Note that the pressure reference point is here chosen at the ambient pressure (taken as zero).

The pressure excess drives in the vapor film a lubrication flow with a horizontal velocity field,

$$U_v = \frac{1}{2\mu_{vm}}\frac{\partial P_v}{\partial x} z(z - h) + \frac{U_d}{h} z, \tag{4}$$

where μ_v is the vapor dynamic viscosity (an additional subscript "m" for vapor properties is explained below) and U_d is the velocity of a possible drop translation as a whole. The no-slip conditions are herewith implied at both boundaries ($U_v = 0$ at $z = 0$ and $U_v = U_d$ at $z = h$). The volumetric flux $q_v = \int_0^h U_v \mathrm{d}z$ is then expressed as

$$q_v = -\frac{1}{12\mu_{vm}}\frac{\partial P_v}{\partial x} h^3 + \frac{U_d}{2} h. \tag{5}$$

Now, assuming that heat is only transferred by conduction across the film, the local evaporation flux is given by

$$\mathcal{J} = \frac{\lambda_{vm}(T_w - T_i)}{\mathcal{L}\, h}, \tag{6}$$

where λ_v is the vapor thermal conductivity, T_i is the liquid-vapor interface temperature equal to the saturation temperature T_{sat},[19] i.e., $T_i = T_{\text{sat}}$, and $\mathcal{L}$ is the latent heat of vaporization.

Finally, the vapor mass conservation reads (quasi-steady approximation)

$$\frac{\partial}{\partial x}(\rho_{vm} q_v) - \mathcal{J} = 0, \tag{7}$$

where ρ_v is the vapor density.

While the liquid properties (here ρ_ℓ, σ, and $\mathcal{L}$) are defined at $T_l = T_{\text{sat}}$ and are therefore *a priori* constant, the constant vapor properties tacitly implied when writing Eqs. (4)–(7) are rather an assumption similar to elsewhere.[15] Within this assumption, it is reasonable to choose their values as evaluated at the mean temperature $(\overline{T}_w + T_{\text{sat}})/2$ of the vapor layer from the known (see the Appendix) constitutive relations $\mu_v(T)$, $\lambda_v(T)$, and $\rho_v(T)$. Thus, $\overline{\mu}_{vm} = \mu_v\left(\frac{\overline{T}_w + T_{\text{sat}}}{2}\right)$, $\overline{\lambda}_{vm} = \lambda_v\left(\frac{\overline{T}_w + T_{\text{sat}}}{2}\right)$, and $\overline{\rho}_{vm} = \rho_v\left(\frac{\overline{T}_w + T_{\text{sat}}}{2}\right)$. The subscript "m" used with the vapor properties denotes their evaluation at the vertically mean temperature $(T_w(x) + T_{\text{sat}})/2$ (still varying with x), while a bar used with the vapor properties means that in their evaluation the horizontally averaged temperature $\overline{T}_w$ is taken to replace $T_w(x)$ wherever appropriate (hence no dependence on x anymore for the vapor properties with a bar). In such a constant-property approach, the effect of the substrate temperature gradient would remain only in the superheat $\Delta T = T_w(x) - T_{\text{sat}}$ [entering Eq. (6)] varying along x.

However, one may wonder whether the asymmetry of physico-chemical properties introduced by the substrate temperature gradient could not be as important as that of ΔT in Eq. (6), e.g., as far as the drop shape is concerned. To test this conjecture, we shall relax the constant vapor property assumption, albeit just partly. Namely, the vapor properties will still be evaluated at the mean temperature, but now locally at each x, hence the values $\mu_{vm}(x) = \mu_v\left(\frac{T_w(x) + T_{\text{sat}}}{2}\right)$, $\lambda_{vm}(x) = \lambda_v\left(\frac{T_w(x) + T_{\text{sat}}}{2}\right)$, and $\rho_{vm}(x) = \rho_v\left(\frac{T_w(x) + T_{\text{sat}}}{2}\right)$. We note that with such vapor properties, dependent on x but not on z, Eqs. (4)–(7) still remain valid.

Combining Eq. (7) with Eqs. (3), (5), and (6) yields the following equation for the film thickness:

$$\frac{1}{12}\frac{\partial}{\partial x}\left[\rho_{vm}\left(\frac{h^3}{\mu_{vm}}\left(\rho_\ell g\frac{\partial h}{\partial x} + \sigma\frac{\partial \kappa}{\partial x}\right) + 6hU_d\right)\right] - \frac{\lambda_{vm}\Delta T}{\mathcal{L}h} = 0, \tag{8}$$

where the curvature κ is given by

$$\kappa = \frac{\frac{\partial^2 h}{\partial x^2}}{\left(1+\left(\frac{\partial h}{\partial x}\right)^2\right)^{3/2}} \tag{9}$$

(for later convenience, no usual simplification to $\kappa = \partial_{xx} h$ is used).

For comparison, in order to stress the role of the temperature dependence of vapor properties, we shall also consider a constant-property version of Eq. (8) given by

$$\frac{1}{12}\frac{\partial}{\partial x}\left(h^3\left(\rho_\ell g\frac{\partial h}{\partial x}+\sigma\frac{\partial \kappa}{\partial x}\right)\right)+\frac{1}{2}\overline{\mu}_{vm}\frac{\partial h}{\partial x}U_d-\frac{\overline{\mu}_{vm}\overline{\lambda}_{vm}\Delta T}{\overline{\rho}_{vm}\mathcal{L}h}=0. \tag{10}$$

Next we turn to boundary conditions. They are specified at the patching points $x = -R_p^l$ and $x = R_p^r$. At each of them, we require the continuity of $h(x)$, $\partial_x h(x)$, and $\kappa(x)$ between the film solution governed by Eqs. (8) and (9) [or by Eqs. (10) and (9)] and the upper shape of the drop already calculated for a given value of $R_{\max}$ in Sec. II A. These six boundary conditions for just two second-order differential equations [Eqs. (8) and (9) or Eqs. (10) and (9)] clearly lead to an overdetermination (two excessive conditions), used, on the one hand, to determine the yet unknown value of h_{elev}. On the other hand, it is also used in the following way. As already mentioned, the asymmetry due to the substrate temperature gradient is expected to make it necessary of using asymmetric patching points, with generally $R_p^l \neq R_p^r$. One of the two, say the right one (the value of R_p^r), can be chosen arbitrarily sufficiently far into the upper (equilibrium) part of the drop (see Fig. 2). Such a degree of arbitrariness goes along with the very notion of introducing patching points and must be verified *a posteriori* to only weakly affect the final results. But then the left one (the value of R_p^l) must be calculated in order to ensure all the mentioned continuities. In this sense, the availability of a second excessive condition above reflects the presence of such yet another unknown R_p^l and confirms the necessity of considering $R_p^l \neq R_p^r$. At last, it is clear that the continuity of the derivatives of a sufficiently high order cannot be imposed due to the approximative nature of a patching-point scheme, and here this starts from the third derivative $\partial_{xxx} h$ (i.e., $\partial_x \kappa$). The underlying approximation is just as good as the influence of the choice of the patching point on the results is weak.

Note also that with all the continuity conditions imposed above, the pressure given by Eq. (3) is automatically continuous through the patching points. Thus, given that in our scheme we have $P_v = 0$ (ambient pressure) for $x < -R_p^l$ and $x > R_p^r$ (equilibrium static shape beyond the patching points), P_v attains the value $P_v = 0$ at both $x = -R_p^l$ and $x = R_p^r$ from the side of the vapor film too.

C. Drop motion

In order to close the formulation, another equation is required to account for the presence of the last unknown U_d. This is accomplished by means of the horizontal balance of forces acting on the drop. In the framework of our approach, the horizontal forces are exerted in the vapor film only (but not over the upper part of the drop). In view of the assumed quasi-steadiness, the net horizontal force must vanish. Thus, we arrive at

$$-\int_{-R_p^l}^{R_p^r}\left(\mu_{vm}\left.\frac{\partial U_v}{\partial z}\right|_{z=h}+P_v\frac{\partial h}{\partial x}\right)\mathrm{d}x=0. \tag{11}$$

Two terms are present in the integral. The first term represents the viscous shear stress exerted by the vapor flow on the drop surface. The second term is due to the action of the normal stress on a curved drop surface. The expressions are consistent at the leading order of the lubrication approximation used here. The integral is taken between the two patching points.

Using Eq. (4) in Eq. (11) leads to

$$-\int_{-R_p^l}^{R_p^r}\left(\frac{1}{2}\frac{\partial P_v}{\partial x}h+P_v\frac{\partial h}{\partial x}\right)\mathrm{d}x-U_d\int_{-R_p^l}^{R_p^r}\frac{\mu_{vm}}{h}\mathrm{d}x=0. \tag{12}$$

However, a surprising setback encountered in Eq. (12) is that the first integral on the left-hand side vanishes identically (while the second obviously does not as its integrand is always positive), thus giving rise to $U_d = 0$ even for asymmetric distributions of P_v and h due to the substrate temperature gradient. Indeed, integrating by parts and taking into account that $P_v = 0$ at both $x = -R_p^l$ and $x = R_p^r$ (see Sec. II B), we obtain $\int_{-R_p^l}^{R_p^r} \partial_x P_v\, h\, \mathrm{d}x = -\int_{-R_p^l}^{R_p^r} P_v\, \partial_x h\, \mathrm{d}x$, and it remains to show that $\int_{-R_p^l}^{R_p^r} P_v\, \partial_x h\, \mathrm{d}x$ vanishes identically within our scheme. Given that $P_v = 0$ beyond the patching points, for $x < R_p^l$ and $x > R_p^r$ (see Sec. II B), the integral in question can rather be rewritten using symmetric integration limits. Let $R_p \equiv \max(R_p^l, R_p^r)$. Then, $\int_{-R_p^l}^{R_p^r} P_v\, \partial_x h\, \mathrm{d}x = \int_{-R_p}^{R_p} P_v\, \partial_x h\, \mathrm{d}x = 0$, where the latter equality is verified by substituting Eq. (3) together with Eq. (9) in here, performing the integration, and making use of the fact that the points $x = \pm R_p$ belong to the *symmetric* equilibrium static shape (see Sec. II A) of the upper part of the drop.

This failure to predict any motion of the drop even in spite of an imposed temperature gradient goes against physical intuition and makes us rethink certain foundations of our model. The encountered degeneracy might simply mean that the sought effect belongs to the realm of smaller effects left behind our leading-order lubrication approach and patching scheme. However, a closer consideration reveals that yet another simplification has been made along the way, the removal of which could in turn remove the degeneracy and permit us to largely stay within the bounds of the present model.

Indeed, in the paragraph leading to Eq. (8), we have argued for a possible importance of the temperature dependence of vapor properties. Yet just a reasonable simplified treatment of this effect has been adopted, within which the vapor properties, even though variable together with the temperature along the vapor film, are still taken constant in each given cross section. Below we show that the degeneracy in the force balance equation does disappear if the temperature dependence of the properties is considered in full, here including the vertical direction. Nonetheless, we shall not reconsider previous developments such as Eq. (8), where the simplified treatment is expected to work reasonably well. Rather, we shall apply the new full treatment in a targeted way to the appropriate

generalization of Eq. (12), where it is really necessary for the degeneracy removal. This is the objective for the remainder of the present subsection.

Considering fully variable vapor properties, the lubrication equation for the vapor flow rather becomes $-\partial_x P_v + \partial_z(\mu_v\ \partial_z U_v) = 0$. Using the same no-slip boundary conditions as previously mentioned (i.e., $U_v = 0$ at $z = 0$ and $U_v = U_d$ at $z = h$), the vapor velocity profile writes

$$U_v = \frac{\partial P_v}{\partial x}\int_0^z \frac{z}{\mu_v}\mathrm{d}z + \frac{1}{\int_0^h \frac{\mathrm{d}z}{\mu_v}}\left(-\frac{\partial P_v}{\partial x}\int_0^h \frac{z}{\mu_v}\mathrm{d}z + U_d\right)\int_0^z \frac{\mathrm{d}z}{\mu_v}. \tag{13}$$

Consequently,

$$\mu_v \left.\frac{\partial U_v}{\partial z}\right|_{z=h} = \frac{\partial P_v}{\partial x}\left(h - \frac{\int_0^h \frac{z}{\mu_v}\mathrm{d}z}{\int_0^h \frac{\mathrm{d}z}{\mu_v}}\right) + \frac{U_d}{\int_0^h \frac{\mathrm{d}z}{\mu_v}}. \tag{14}$$

Using the quasi-steady thin-film thermal diffusion equation in the vapor layer $\partial_z(\lambda_v \partial_z T) = 0$ with the boundary conditions $T = T_w$ at $z = 0$ and $T = T_{\mathrm{sat}}$ at $z = h$ permits us to express Eq. (14) in terms of T instead of z on account of $\mathrm{d}z = -h\lambda_v \mathrm{d}T / \int_{T_{\mathrm{sat}}}^{T_w} \lambda_v \mathrm{d}T$ as follows:

$$\mu_v \left.\frac{\partial U_v}{\partial z}\right|_{z=h} = \frac{\partial P_v}{\partial x} h\,(1-f) + \mu_{v,\mathrm{eff}}\frac{U_d}{h} \tag{15}$$

with

$$f = \frac{\int_{T_{\mathrm{sat}}}^{T_w} \lambda_v \left(\int_{T_{\mathrm{sat}}}^{T} \frac{\lambda_v \mathrm{d}T'}{\mu_v}\right)\mathrm{d}T}{\left(\int_{T_{\mathrm{sat}}}^{T_w} \lambda_v \mathrm{d}T\right)\left(\int_{T_{\mathrm{sat}}}^{T_w} \frac{\lambda_v \mathrm{d}T}{\mu_v}\right)} \tag{16}$$

and

$$\mu_{v,\mathrm{eff}} = \frac{\int_{T_{\mathrm{sat}}}^{T_w} \lambda_v \mathrm{d}T}{\int_{T_{\mathrm{sat}}}^{T_w} \frac{\lambda_v \mathrm{d}T}{\mu_v}}. \tag{17}$$

Then, rather using Eq. (15) for the viscous shear stress in Eq. (11) and knowing that $\int_{-R_p^l}^{R_p^r} (\partial_x P_v\, h + P_v\, \partial_x h)\mathrm{d}x = [P_v h]_{-R_p^l}^{R_p^r} = 0$ leads to the following expression for the horizontal balance of the forces acting on the drop bottom surface:

$$\int_{-R_p^l}^{R_p^r} \frac{\partial P_v}{\partial x} h f \mathrm{d}x - U_d \int_{-R_p^l}^{R_p^r} \frac{\mu_{v,\mathrm{eff}}}{h}\mathrm{d}x = 0. \tag{18}$$

A key difference of the new treatment manifest in Eq. (18) is the appearance of a factor f inside the integral. As evidenced by Eq. (16), this factor is generally non-constant, $f = f(x)$, once a non-constant substrate temperature $T_w(x)$ is imposed as in our case. With $f = f(x)$, the first term in the left-hand side of Eq. (18) no longer identically vanishes (see also a more concrete example below), and thus, the degeneracy is thereby removed. In contrast, in the framework of the earlier simplified treatment, when λ_v and μ_v were taken constant across the film (i.e., just replaced with λ_{vm} and μ_{vm}, respectively), Eq. (16) simply yields $f = 1/2$, a constant value giving rise to the degeneracy as explained earlier. Importantly, it is the dependence $\mu_v(T)$ that is the key for yielding a non-constant f, and not $\lambda_v(T)$. Indeed, one can see that $\mu_v = \mathrm{const}$ in Eq. (16) would lead to $f = 1/2$ irrespective of $\lambda_v(T)$.

Noting that the ratio λ_v/μ_v is typically almost constant since both properties are similarly varying with the temperature (see the Appendix) as well as the fact that the water data in the temperature range of interest fall well on a linear law $\mu_v = \mu_{v,\mathrm{ref}} + \mu_{v\mathrm{T}}(T - T_{\mathrm{ref}})$, where $\mu_{v\mathrm{T}}$ is a constant, one can simplify Eqs. (16) and (17) to

$$f \approx \frac{1}{2} + \frac{1}{12}\frac{\mu_{v\mathrm{T}}(T_w - T_{\mathrm{sat}})}{\mu_{vm}} \tag{19}$$

and

$$\mu_{v,\mathrm{eff}} \approx \mu_{vm} \tag{20}$$

which will be used in this form in the remainder of the paper.

It is interesting to note that Eq. (18) clearly highlights two forces acting on the drop horizontally. The first term corresponds to the thermal force F_{th}, a propulsion force originating from the thermal gradient $\partial_x T_w$. The second term in Eq. (18) is clearly the viscous drag force F_{vis} exerted by the shear stress in the vapor layer, due to the drop translation. Note that in all generality F_{th} is a function of not only its primary factor $\partial_x T_w$ but also of U_d, whereas F_{vis} is a function of not only its primary factor U_d but also of $\partial_x T_w$. This comes from the nonlinear effects due to the vapor film shape dependence on both factors.

The sign of the viscous drag force F_{vis} is immediately obvious from Eq. (18): it is just opposite to the sign of the drop velocity U_d, as expected on physical grounds. It is less obvious that the sign of the thermal propulsion force F_{th} can in fact already be anticipated as well from the following simple considerations. On account of the degeneracy ($F_{\mathrm{th}} \equiv 0$ should f be spatially constant), it is only a non-constant part of f that matters. The vapor dynamic viscosity μ_v being an increasing function of temperature, f is expected to be larger where the substrate is hotter, and smaller where the substrate is colder. Furthermore, for the lubrication vapor flow, one must predominantly have $\partial_x P_v < 0$ in the right part of the drop, and $\partial_x P_v > 0$ in the left part. As a result of all this, the force F_{th} [the first term of Eq. (18)] can be seen to be directed, and hence the drop must move, towards the colder region of the substrate. This conjecture will be confirmed by concrete computations later on. The physical interpretation, compatible with (and actually based on) the degeneracy and the developments given by Eqs. (13)–(17), ultimately turns out to be rather straightforward. Namely, under otherwise equal conditions (viz., the pressure gradient and vapor film thickness), the vapor flow tends to be more intense in the colder part, where the dynamic viscosity is lower. At the same time, the dynamic viscosity of the vapor at the drop surface is always the same, as defined at the temperature $T_i = T_{\mathrm{sat}}$. Therefore, the viscous shear stress exerted upon the drop is predominant in the colder direction, which is where the drop is eventually entrained by the vapor flow.

This completes the formulation initiated in Secs. II A and II B. To sum-up, the upper part of the Leidenfrost drop, down to the patching points at the left and right vapor outlets, is treated as an equilibrium static shape as described in Sec. II A. The vapor layer and the conditions at the asymmetric patching points are treated as described in Sec. II B, where the lubrication equation is given by Eq. (8) assuming partial variability of vapor properties (in the x direction only). The closure to the formulation at the level of a horizontal force balance is given by Eq. (18) with Eqs. (3), (19), and (20), where we had to assume the full variability of vapor properties in order to get rid of the degeneracy. This model, referred to as the *complete*

model in what follows, is solved numerically by using a standard second-order finite-difference scheme on a uniform grid and applying the Newton-Raphson method.

For comparison, a simplified version of the complete model was also proposed with the only difference that the lubrication equation, Eq. (8), with x-dependent vapor properties is replaced by Eq. (10) corresponding to fully constant vapor properties. Note that the constancy of vapor properties here applies only to the lubrication equation. Yet, in view of the otherwise emerging degeneracy, we still have to keep as the closure given by Eq. (18) with Eqs. (3), (19), and (20) implying the full variability of vapor properties. This model will be referred to as the *model with constant properties in the lubrication equation*.

D. The limit of weak asymmetry

In a theoretical analysis like ours,[15] the Leidenfrost state can exist down to arbitrarily small positive values of ΔT. However, in reality, it is never observed for drops over flat solid substrates at ΔT smaller than several tens of degrees. While the problem of such Leidenfrost threshold still awaits its resolution, this means in the present context that our analysis is practically applicable only to such large values of $\overline{\Delta T} = \overline{T}_w - T_{\mathrm{sat}}$. On the other hand, one can hardly expect substrate temperature gradients and the corresponding temperature differences $\Delta T_w = T_w^r - T_w^l$ underneath a drop of at most several millimeters to be that large. Thus, $\Delta T_w \ll \overline{\Delta T}$ appears as quite a practical case to be considered, which we shall do in the present subsection.

The case $\Delta T_w \ll \overline{\Delta T}$ also implies that the local superheats $(T_w^l - T_{\mathrm{sat}})$ and $(T_w^r - T_{\mathrm{sat}})$ at the two ends of the drop differ only insignificantly in relative terms. It is therefore clear that the drop asymmetry (more precisely, that of its bottom surface, associated with the vapor layer, for the upper part of the drop is always treated as symmetric in our present scheme) must then be weak. If all relevant quantities are now represented as a sum of a symmetric part (marked with a subscript 0) and the remaining asymmetric part (marked with a prime) as $T_w = T_{w0} + T_w'$, $\Delta T = \Delta T_0 + \Delta T'$, $h = h_0 + h'$, $\kappa = \kappa_0 + \kappa'$, $P_v = P_{v0} + P_v'$, $\mu_v = \mu_{v0} + \mu_v'$, $\lambda_v = \lambda_{v0} + \lambda_v'$, $\rho_v = \rho_{v0} + \rho_v'$, $\mu_{vm} = \mu_{vm0} + \mu_{vm}'$, $\lambda_{vm} = \lambda_{vm0} + \lambda_{vm}'$, $\rho_{vm} = \rho_{vm0} + \rho_{vm}'$, $f = f_0 + f'$, $R_p^l = R_{p0}^l + R_p^{l'}$, $R_p^r = R_{p0}^r + R_p^{r'}$, etc., the asymmetric parts will then just be a small correction over the symmetric ones. Obviously, we can use $T_{w0} = \overline{T}_w$, $\Delta T_0 = \overline{\Delta T}$, $\mu_{v0} = \overline{\mu}_v$, $\lambda_{v0} = \overline{\lambda}_v$, $\rho_{v0} = \overline{\rho}_v$, $\mu_{vm0} = \overline{\mu}_{vm}$, $\lambda_{vm0} = \overline{\lambda}_{vm}$, $\rho_{vm0} = \overline{\rho}_{vm}$, and $f_0 = \overline{f}$. In the spirit of earlier introduced definitions (see Sec. II B), the bar here refers by definition to characteristics that would be obtained at a constant substrate temperature $T_w \equiv \overline{T}_w$. Note also that, in accordance with the last but one paragraph of Sec. II B, we can choose $R_p^{r'} \equiv 0$ without loss of generality.

The symmetric part of the solution will be explicitly required in what follows. The solution for $h_0(x)$ and $\kappa_0(x)$ is obtained in the same way as described in Sec. II B, with a simplification of certain aspects of the solution procedure on account of symmetry. In particular, Eqs. (10) and (9) hold, where one must now introduce the quantities $h = h_0$, $\kappa = \kappa_0$, and $\Delta T = \overline{\Delta T}$, as well as $U_d = 0$. We also note that Eq. (3) is still valid in terms of the symmetric quantities h_0, κ_0, and P_{v0}. The patching point is now realized in terms of symmetric patching points $R_{p0}^l = R_{p0}^r \equiv R_{p0}$, or rather the problem can now be formulated just in a half-interval $0 < x < R_{p0}$ using the symmetry conditions $\partial_x h_0 = 0$ and $\partial_x \kappa_0 = 0$ at $x = 0$. Needless to say that no horizontal force balance like considered in Sec. II C is required within the (symmetric) problem for h_0 and κ_0, for it is trivially satisfied (with $U_d = 0$). The present symmetric solution is a full planar counterpart of the axisymmetric solution obtained elsewhere.[15]

We next turn to the central point of the present subsection, which concerns an essential simplification of the force condition given by Eq. (18) in the weak asymmetry limit. Indeed, linearizing Eq. (18) about the symmetric solution, we arrive at

$$\int_{-R_{p0}}^{R_{p0}} \frac{\partial P_{v0}}{\partial x} h_0 f' \mathrm{d}x - \overline{\mu}_{vm} U_d \int_{-R_{p0}}^{R_{p0}} \frac{\mathrm{d}x}{h_0} = 0. \tag{21}$$

The fact that the second term on the left-hand side of Eq. (21) depends only on the symmetric solution (apart from the factor U_d) is a straightforward consequence of the linearization, given that U_d is just a small asymmetric parameter in this scheme. However, the same fact about the first term is less trivial and quite remarkable, where we note that f' is expressible beforehand from the linearization of either Eq. (16) or Eq. (19) as $f' = (\partial_{T_w} f|_{T_w = \overline{T}_w}) T_w'$. Indeed, all other possible linearization contributions (containing h', P_v', $R_p^{l'}$, and with $\overline{f}$ = const in the place of f) into the first term identically vanish in view of the degeneracy discussed in Sec. II C. Thus, as manifest in Eq. (21), the horizontal force balance and the drop velocity U_d can remarkably be expressed using the symmetric solution only, if working in the limit of the weak asymmetry.

In view of Eq. (21), the forces F_{th} and F_{vis} (see the end of Sec. II C) can now be expressed just as linear functions of the corresponding primary factors,

$$F_{\mathrm{th}} = -\alpha_{\mathrm{th}} A_w, \tag{22}$$

$$F_{\mathrm{vis}} = -\alpha_{\mathrm{vis}} U_d, \tag{23}$$

with the coefficients

$$\alpha_{\mathrm{th}} = -\frac{\mu_{vi}\mu_{v\mathrm{T}}}{6\overline{\mu}_{vm}^2} \int_0^{R_{p0}} \frac{\partial P_{v0}}{\partial x} h_0 x \mathrm{d}x, \tag{24}$$

$$\alpha_{\mathrm{vis}} = 2\overline{\mu}_{vm} \int_0^{R_{p0}} \frac{\mathrm{d}x}{h_0} \tag{25}$$

that depend on neither A_w nor U_d and are calculated from the symmetric profiles $h_0(x)$ and $P_{v0}(x)$ only. In Eqs. (22) and (24), we assumed a linear temperature profile $T_w' = A_w x$ as well as the simplification of the f expression given by Eq. (19), which yields $f' = \frac{\mu_{vi}\mu_{v\mathrm{T}}}{12\overline{\mu}_{vm}^2} T_w'$ with $\mu_{vi} = \mu_v(T_i = T_{\mathrm{sat}})$. The force balance given by Eq. (21) rewrites in these terms as

$$F_{\mathrm{th}} + F_{\mathrm{vis}} = 0, \tag{26}$$

yielding the result

$$U_d = -\frac{\alpha_{\mathrm{th}}}{\alpha_{\mathrm{vis}}} A_w \tag{27}$$

for the drop migration velocity induced by the temperature gradient.

The sign of F_{vis} as a drag force given by Eqs. (23) and (25) is expectedly opposite to that of U_d, as already discussed in Sec. II C. Indeed, note that $\alpha_{\text{vis}} > 0$. Likewise, the sign of F_{th}, viz., of α_{th}, is as anticipated in Sec. II C. Now this is seen even more unambiguously. Indeed, the symmetric vapor pressure P_{v_0} must clearly satisfy $\partial_x P_{v_0} < 0$ for $0 < x < R_p$. Then $\alpha_{\text{th}} > 0$, as evidenced by Eq. (24). Thus the drop will drift against the applied temperature gradient, towards the colder regions.

Thus, the linearization undertaken in the present subsection has permitted to effectively represent the horizontal forces acting on the Leidenfrost drop and express its velocity based on the symmetric vapor film profiles (in the absence of substrate temperature gradient) only. Such a *linearized* result for the velocity, Eq. (27), will be compared in Sec. III with the corresponding *complete* result based on the formulation of Sec. II C without resorting to any linearization. On the other hand, the linearization will not be further pursued in the present paper as far as the computation of the asymmetric parts of the solution (with a prime) is concerned. When interested in the asymmetric vapor film profiles, we shall rather proceed from the complete formulation given in Secs. II B and II C.

E. Dimensionless parameters

Hereafter, it will be convenient to represent certain results in dimensionless form for the sake of universality. The dimensionless quantities will be marked by a tilde. All the lengths are normalized with the capillary length $\ell_c = (\sigma/\rho_\ell g)^{1/2}$. In dimensionless form, the coefficients (24) and (25) can be rendered as

$$\tilde{\alpha}_{\text{th}} = \frac{6\overline{\mu}_{vm}^2 \alpha_{\text{th}}}{\sigma_\ell \ell_c \mu_{vi} \mu_{v\text{T}}} = -\int_0^{\tilde{R}_{p_0}} \frac{\partial \tilde{P}_{v_0}}{\partial \tilde{x}} \tilde{h}_0 \tilde{x} \mathrm{d}\tilde{x}, \tag{28}$$

$$\tilde{\alpha}_{\text{vis}} = \frac{\alpha_{\text{vis}}}{2\overline{\mu}_{vm}} = \int_0^{\tilde{R}_{p_0}} \frac{\mathrm{d}\tilde{x}}{\tilde{h}_0}, \tag{29}$$

which must remarkably be functions of only two dimensionless parameters: the drop size $\tilde{R}_{\max}$ and the evaporation number $\mathcal{E} = \frac{\overline{\lambda}_{vm}\overline{\mu}_{vm}\overline{\Delta T}}{\overline{\rho}_{vm}\sigma_\ell \ell_c \mathcal{L}}$ (as the overall Leidenfrost shape is found to be in the case of an isothermal substrate within our approach[15]). Note that there is no difference in this regard between the axisymmetric case considered in Ref. 15 and the present 2D case in terms of $\tilde{h}_0$: the non-dimensionalization of the corresponding formulation can be repeated *verbatim* giving rise to the same exhaustive list of two dimensionless parameters $\tilde{R}_{\max}$ and $\mathcal{E}$. The dimensionless excess of pressure is introduced as $\tilde{P}_{v_0} = (\ell_c/\sigma)P_{v_0}$. On account of Eq. (3), this yields $\partial_{\tilde{x}}\tilde{P}_{v_0} = -\partial_{\tilde{x}}\tilde{h}_0 - \partial_{\tilde{x}}\tilde{\kappa}_0$ which is to be used in Eq. (28), where $\tilde{\kappa}_0 = \partial_{\tilde{x}\tilde{x}}\tilde{h}_0/(1+(\partial_{\tilde{x}}\tilde{h}_0)^2)^{3/2}$ in accordance with Eq. (9).

With (28) and (29), the result (27) for the drop velocity can be rewritten as

$$U_d = -\frac{\sigma_\ell \ell_c \mu_{vi}\mu_{v\text{T}}}{12\overline{\mu}_{vm}^3} \frac{\tilde{\alpha}_{\text{th}}}{\tilde{\alpha}_{\text{vis}}} A_w, \tag{30}$$

where it now remains to express $\tilde{\alpha}_{\text{th}}/\tilde{\alpha}_{\text{vis}}$ as a function of $\tilde{R}_{\max}$ and $\mathcal{E}$ for a universal representation.

We note that in the general case of f, not limited to Eq. (19), the results given by Eqs. (22)–(30) are just modified by using $\partial_{T_w} f$ at $T_w = \overline{T}_w$ as calculated from Eq. (16) in lieu of the multiplier $\frac{\mu_{vi}\mu_{v\text{T}}}{12\overline{\mu}_{vm}^2}$. Note also that the dimensionless coefficients $\tilde{\alpha}_{\text{vis}}$ and $\tilde{\alpha}_{\text{th}}$ remain hereby unchanged and are thus universal in this sense.

III. RESULTS AND DISCUSSION

A. Drop geometry

Figure 3 presents numerically predicted shapes of moving 2D Leidenfrost water drops. The substrate underneath the drop has an average temperature $\overline{T}_w = 300\,^\circ\text{C}$ (i.e., $\overline{\Delta T} = 200\,^\circ\text{C}$), and a thermal gradient $A_w = -2$ K/mm is applied. The vapor film is seen to be composed of a vapor pocket surrounded by two necks, similarly to the case of motionless axisymmetric drops over an isothermal substrate.[15–18] However, in the present situation when the substrate is subject to a thermal gradient, the bottom drop surface is asymmetric. Indeed, even if hardly discernible by the eye, the thicknesses of the vapor layer at the two neck locations are in fact different. For a drop of $R_{\max} = \ell_c$ [see Fig. 3(a)], we have $h^l_{\text{neck}} = 59.22$ μm and $h^r_{\text{neck}} = 58.79$ μm. For a drop of $R_{\max} = 2\ell_c$ [see Fig. 3(b)], we obtain $h^l_{\text{neck}} = 72.23$ μm and $h^r_{\text{neck}} = 70.68$ μm. The thickness differences at the neck locations $\Delta h_{\text{neck}} = h^r_{\text{neck}} - h^l_{\text{neck}}$ are then -0.43 μm and -1.56 μm, respectively. The predicted asymmetry is quite small, indeed, but grows with the drop size. As expected, h_{neck} is larger at the location where the substrate is hotter. Indeed, it was previously shown[15,17] that we roughly have $h_{\text{neck}} \sim (T_w - T_{\text{sat}})^{1/3}$. Therefore, the

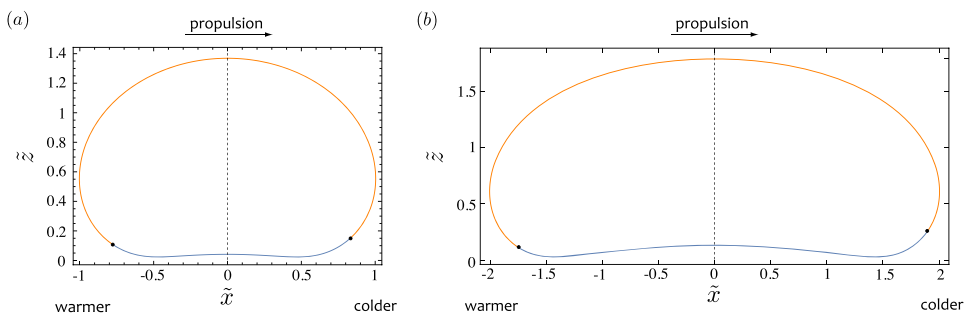

FIG. 3. Shapes of moving 2D Leidenfrost water drops of dimensionless sizes $\tilde{R}_{\max} = 1$ (a) and $\tilde{R}_{\max} = 2$ (b) on a substrate with an average temperature $\overline{T}_w = 300\,^\circ\text{C}$ ($\overline{\Delta T} = 200\,^\circ\text{C}$) and a thermal gradient $A_w = -2$ K/mm computed by the complete model (see the end of Sec. II C). The orange line represents the upper part (equilibrium) solution for the drop shape, whereas the blue one results from the lubrication theory for the vapor film. One can observe that the patching points (represented by dots) are asymmetric, although the asymmetry is hardly discernable in the vapor film profile. $\tilde{x}$ and $\tilde{z}$ are the coordinates made dimensionless by the capillary length of the drop (i.e., 2.5 mm for water at T_{sat}).

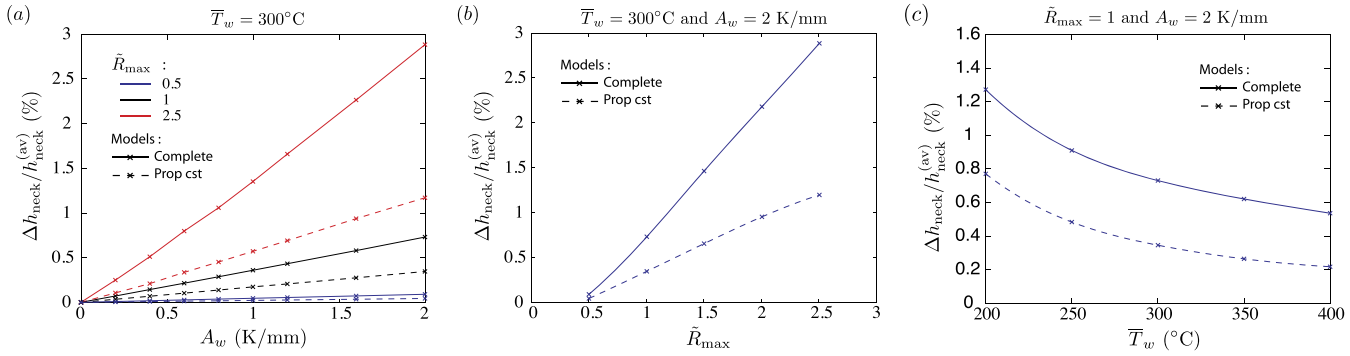

FIG. 4. Asymmetry of the bottom drop surface $\Delta h_{neck}/h_{neck}^{(av)}$ for a moving 2D Leidenfrost water drop as a function of (a) the substrate thermal gradient for a number of drop sizes and for $\overline{T}_w = 300\,°C$ (i.e., $\overline{\Delta T} = 200\,°C$), (b) the drop size for $\overline{T}_w = 300\,°C$ and $A_w = 2$ K/mm, and (c) the average substrate temperature for $\tilde{R}_{max} = 1$ and $A_w = 2$ K/mm. The complete model (solid lines) is compared with the one assuming constant vapor properties in the lubrication equation (dashed lines). The drop radius is normalized with the capillary length (i.e., 2.5 mm for water at T_{sat}).

drop bottom appears to be slightly tilted towards the colder region.

Figure 4 shows the asymmetry of the bottom drop surface, measured in terms of $\Delta h_{neck}/h_{neck}^{(av)} = 2\,(h_{neck}^r - h_{neck}^l)/(h_{neck}^r + h_{neck}^l)$, i.e., the relative thickness difference at the two neck locations, as a function of the substrate thermal gradient A_w, the drop size $\tilde{R}_{max}$, and the substrate average temperature $\overline{T}_w$. The figure highlights that the asymmetry of the bottom drop surface (i.e., $\Delta h_{neck}/h_{neck}^{(av)} \neq 0$) develops as soon as $A_w \neq 0$. The asymmetry $\Delta h_{neck}/h_{neck}^{(av)}$ appears to increase both with the thermal gradient A_w and with the drop size $\tilde{R}_{max}$. Indeed, $\Delta h_{neck}/h_{neck}^{(av)} \sim [(T_w^r - T_{sat})^{1/3} - (T_w^l - T_{sat})^{1/3}]/(\overline{T}_w - T_{sat})^{1/3}$ increases with the difference of the substrate temperature at the neck locations $(T_w^r - T_w^l)$ for a constant $\overline{T}_w$. On the contrary, $\Delta h_{neck}/h_{neck}^{(av)}$ slightly decreases with an increase in $\overline{T}_w$. Note that for a given ΔT, the necks/pocket structure of the drop bottom disappears for a small drop size.[15,17] Figure 4 also compares results of our complete model, based on Eq. (8), with the ones of the model assuming constant vapor properties in the lubrication equation, based on Eq. (10). The difference between the two is quite appreciable. The contribution of the temperature dependence of vapor properties, as retrieved in Eq. (8), into the asymmetry proves to be rather significant. For example, the asymmetry of the bottom drop surface is about three times more important when calculated with the complete model than when calculated with constant vapor properties in the lubrication equation for $A_w = 2$ K/mm, $\tilde{R}_{max} = 2.5$, and $\overline{T}_w = 300\,°C$. Finally, it is worth noting that the asymmetry of the bottom drop surface is relatively small. It is at most of the order of 3% in the studied parameter range. Note that it corresponds to an apparent angle $\beta = (h_{neck}^l - h_{neck}^r)/(R_{neck}^l + R_{neck}^r)$ of the order of 0.012°.

B. Drop motion

Figure 5 shows the velocity U_d of a 2D Leidenfrost water drop as a function of the substrate thermal gradient A_w, drop size $\tilde{R}_{max}$, and average temperature of the substrate $\overline{T}_w$. First, it is worth noticing that the value of the velocity is negative, $U_d < 0$, for $A_w > 0$. Consequently, the drop turns out to move in the direction opposite to the thermal gradient, i.e., towards the colder region of the substrate, as it was already anticipated. Thus, a Leidenfrost drop on a substrate with a thermal gradient self-propels in the direction of closing angles, as in the case of the platelet of dry ice with a small weight on a flat isothermal substrate [see Fig. 1(c)]. The computed velocities are of the order of a few mm/s. Except for large

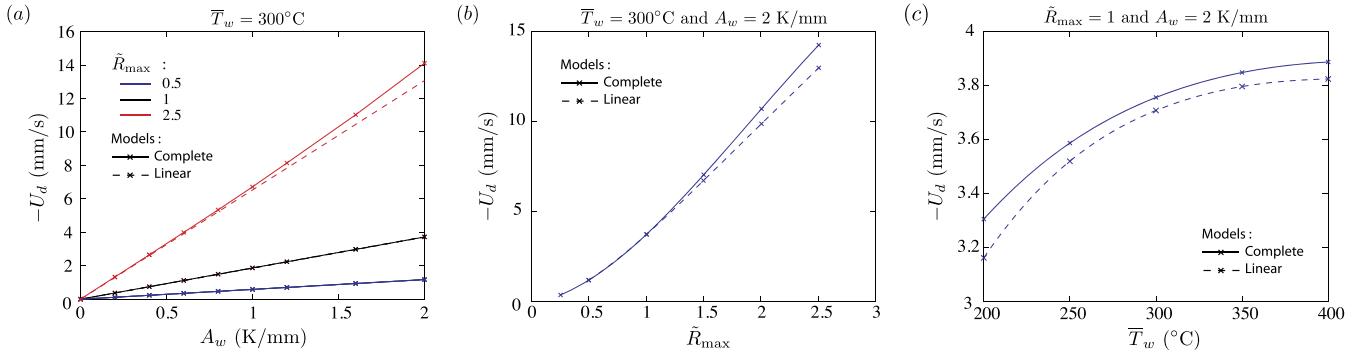

FIG. 5. Velocity of a 2D Leidenfrost water drop U_d as a function of (a) the substrate thermal gradient A_w for several dimensionless drop sizes $\tilde{R}_{max}$ and an average substrate temperature of $\overline{T}_w = 300\,°C$, (b) the drop size for $\overline{T}_w = 300\,°C$ and $A_w = 2$ K/mm, and (c) the average substrate temperatures for $\tilde{R}_{max} = 1$ and $A_w = 2$ K/mm. The complete model (solid lines) is compared with the linearized one (dashed lines). The drop radius is normalized with the capillary length (i.e., 2.5 mm for water at T_{sat}).

thermal gradients, this is generally slower than in the case of Leidenfrost drops moving on isothermal ratchets where drop velocities of a few cm/s were reported. For instance, here, a 2D Leidenfrost water drop of size $\tilde{R}_{\max} = 2.5$ can reach a velocity of about 14 mm/s on a substrate with an average temperature $\overline{T}_w = 300\,^{\circ}\mathrm{C}$ subject to a thermal gradient of 2 K/mm.

Figure 5 reveals that the value of the drop velocity increases with all the three parameters considered. However, while the drop velocity proves to be strongly influenced by the substrate thermal gradient A_w and the drop size $\tilde{R}_{\max}$, it is only weakly dependent on the average temperature of the substrate $\overline{T}_w$. It is worth noticing that the drop velocity increases almost linearly with A_w, as predicted by the linearized version of our model [see Eqs. (27) and (30)].

Indeed, Fig. 5 also compares results of our complete model with the ones of the linearized version of the model. A good agreement between the two is observed. Thus, the linearized model appears to properly depict the self-propulsion of a 2D Leidenfrost drop on a substrate subject to not so large thermal gradients. Then, it is interesting to note that, to evaluate the drop velocity, there is actually no need of computing its asymmetric shape. Rather, as pointed out in Sec. II D and Eqs. (27) and (30), this can merely be carried out using its symmetric Leidenfrost shape, predicted for an isothermal substrate ($A_w = 0$). Furthermore, such a linearized treatment offers a physically intuitive insight in terms of the (horizontal) forces acting on our Leidenfrost drop.

C. Forces acting on the drop

The linearized model presented in Sec. II D highlights the two forces acting on the drop: the propulsion force F_{th}, which is proportional to the substrate thermal gradient A_w [see Eq. (22)], and the drag force F_{vis}, which is proportional to the drop velocity U_d [see Eq. (23)]. Figures 6(a)–6(d) show the values of the dimensionless linear coefficients $\tilde{\alpha}_{\mathrm{th}}$ and $\tilde{\alpha}_{\mathrm{vis}}$ [calculated from the symmetric solution, see Sec. II E and Eqs. (28) and (29)] as functions of the only two parameters of the system remaining when rewritten in dimensionless form: the evaporation number $\mathcal{E}$ and the drop size

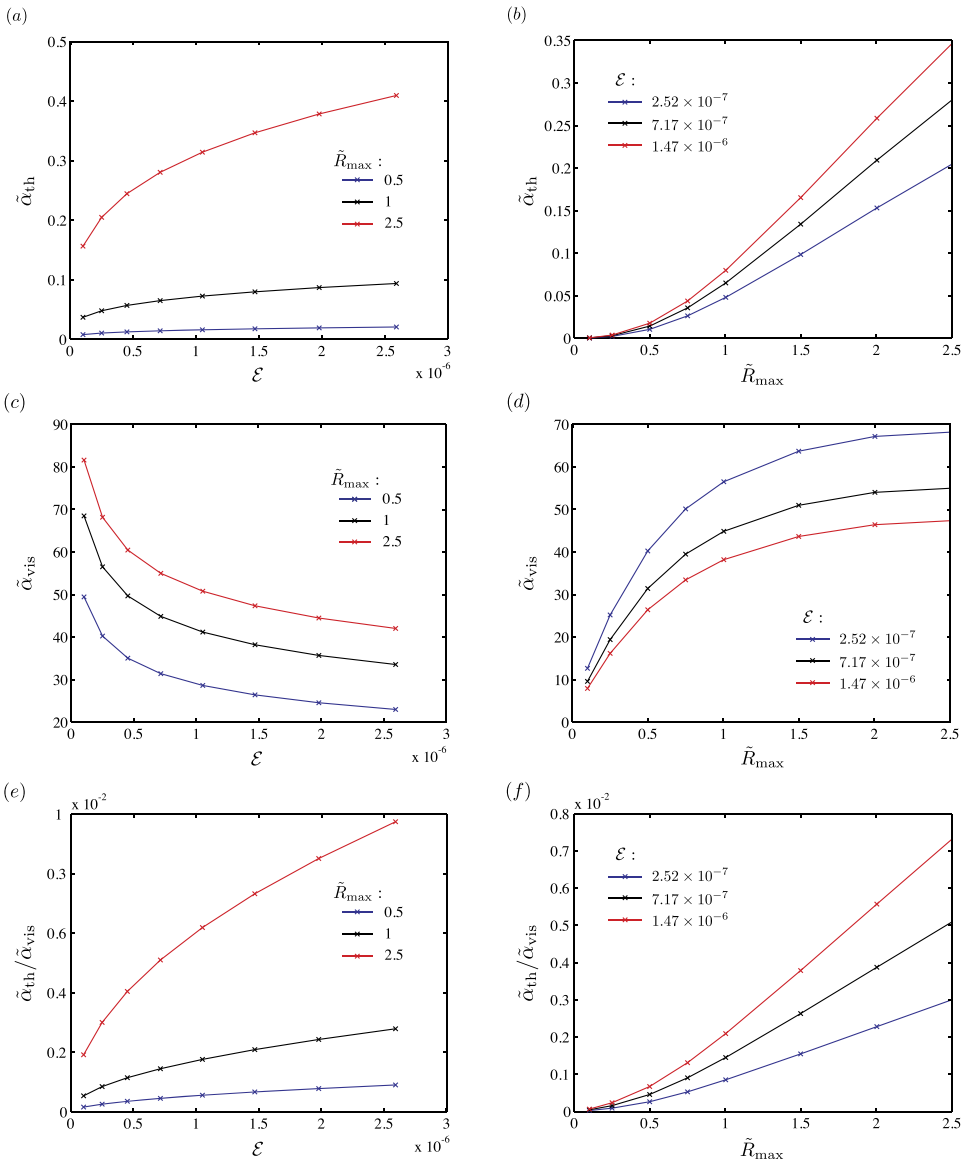

FIG. 6. Dimensionless linear coefficients of the thermal (propulsion) and viscous (drag) forces as functions of the evaporation number for various drop sizes [(a) and (c), respectively] and of the drop size for various evaporation numbers [(b) and (d), respectively]. [(e) and (f)] Ratio of the two linear coefficients, determining the drop velocity [see Eq. (30)], as a function of the two dimensionless numbers. Note that the various considered values of $\mathcal{E}$ in [(b), (d), and (f)] (i.e., $\mathcal{E} = [2.52 \times 10^{-7};\ 7.17 \times 10^{-7};\ 1.47 \times 10^{-6}]$ correspond to water for an average substrate temperature $\overline{T}_w = [200;\ 300;\ 400]\,^{\circ}\mathrm{C}$, respectively).

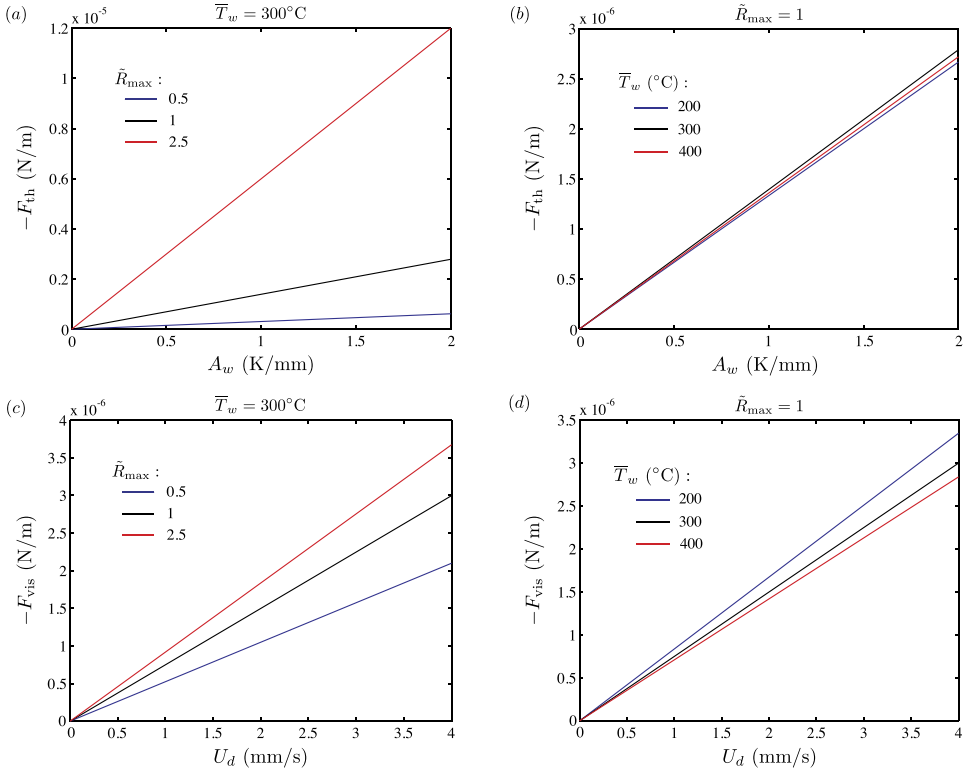

FIG. 7. [(a) and (b)] Thermal (propulsion) force as a function of the substrate thermal gradient for (a) various drop sizes and $\overline{T}_w = 300\,°C$, and (b) various average substrate temperatures and $\tilde{R}_{max} = 1$. [(c) and (d)] Viscous (drag) force as a function of the drop velocity for (c) various drop sizes and $\overline{T}_w = 300\,°C$, and (d) various average substrate temperatures and $\tilde{R}_{max} = 1$. All according to the linearized model.

$\tilde{R}_{max}$ (defined in Sec. II E). The values of both linear coefficients increase with $\tilde{R}_{max}$. However, while $\tilde{\alpha}_{th}$ increases with $\mathcal{E}$, $\tilde{\alpha}_{vis}$ decreases with $\mathcal{E}$. Figures 6(e) and 6(f) show the ratio of the two linear coefficients as a function of the two dimensionless parameters. Recall that it is the ratio $\tilde{\alpha}_{th}/\tilde{\alpha}_{vis}$ that actually links the drop velocity to the substrate thermal gradient [see Eq. (30)]. It is interesting to note that the ratio increases with both the evaporation number $\mathcal{E}$ and the drop size $\tilde{R}_{max}$.

Finally, Fig. 7 enables appreciating the actual orders of magnitude of the two horizontal forces (F_{th} and F_{vis}) acting on the drop in the framework of the linearized approach (valid for not too large A_w and U_d). They both prove to be of the order of 10^{-6}–10^{-5} N/m in the parameter range studied. ($-F_{th}$) obviously increases (linearly) with the substrate thermal gradient. This force also increases with the drop size. The value of the average substrate temperature does not appear really to affect this propulsion force. Concerning F_{vis}, it obviously increases (linearly) with the drop velocity. This force also increases with the drop size but decreases when the average substrate temperature increases, the latter apparently due to an increase in the vapor film thickness reducing the viscous drag.

IV. CONCLUSIONS AND PERSPECTIVES

We have theoretically studied the behavior of a Leidenfrost drop over a flat rigid horizontal substrate when the substrate is not isothermal but rather has a thermal gradient imposed along its surface. For simplicity, the analysis has been carried out in a 2D planar geometry. Quite expectedly, it has been found that the drop can no longer stay symmetric as in the case of an isothermal substrate, and a slight asymmetry becomes apparent in its shape. Furthermore, due to the overall asymmetry, the drop can no longer remain at rest and rather self-propels in a preferential direction. We have found that the bottom surface of the drop slightly tilts towards the colder side of the substrate, the neck being naturally slightly thinner where the substrate is colder. Moreover, it is towards the colder side too (i.e., against the applied thermal gradient and in the direction of the closing angle) that the drop self-propels. In particular, a centimetric water drop can reach velocities of the order of 1 cm/s for thermal gradients of the order of a few K/mm, the value depending only slightly on the superheat. Thus, substrate temperature heterogeneities could potentially be considered as an alternative way of generating self-propulsion of Leidenfrost drops, e.g., in view of microfluidics applications.

On the methodological side, the approach applied in Ref. 15 (lubrication vapor film patched to an equilibrium upper part of the drop) proved to work well in the present asymmetric situation too, giving rise to asymmetric vapor film and patching points, yet with a symmetric upper part of the drop. Interestingly, we have found that the vapor properties asymmetry due to their temperature dependence contributes significantly (roughly by half) to the resulting drop shape asymmetry. The temperature dependence of the vapor properties is therefore an important factor worth to be retained in the formulation. Even more strikingly, we have revealed a peculiar degeneracy occurring in the framework of our approach. Namely, even with the overall asymmetry due to the applied thermal gradient, the computation of the horizontal force acting on the drop (the sum of the viscous shear and the horizontal pressure projection on the vapor film profile) yields an identically vanishing result, unless the temperature dependence

of the vapor properties (importantly of its dynamic viscosity) is accounted for in full detail. Note that such an impreative necessity of its taking into account is not what is typically encountered in similar studies throughout the literature. We stress that the property temperature dependence is a real effect in the vapor layer, for the temperature variations across it are as large as the (rather elevated) Leidenfrost superheats typically comparable with the absolute temperature itself. Therefore, the fact that our drop velocity calculation rather unexpectedly hinges, because of the degeneracy, on the vapor viscosity variability with the temperature does not actually belittle the thereby obtained results. On the one hand, sweeping away the inessential details, the degeneracy makes possible the following simple interpretation of the predicted sense of the drop migration. The vapor dynamic viscosity increasing with the temperature, the vapor film flow is less viscous and hence more intense towards the colder side than towards the warmer side. At the same time, the vapor viscosity is the same all along the drop surface finding itself at the saturation temperature. As a result, the viscous shear stress exerted by the vapor flow is predominantly towards the colder region, and it is in this direction that the drop is entrained.

In view of the fact that the asymmetry actually turns out to be small, a linearized version of the model has also been considered. The linearization is accomplished about the state with an isothermal substrate and the corresponding symmetric (i.e., classical) Leidenfrost shape. Quite remarkably, thanks to the mentioned degeneracy, it turns out that there is no need of calculating the actual shape asymmetry in order to calculate the drop velocity induced by the substrate thermal gradient. The classical (symmetric) shape alone just fully suffices for this purpose, which results in a great simplification of the analysis. Such a linearized version has successfully been validated against the full model. The linearized version also permits us to clearly distinguish the two horizontal forces acting on the drop: the thermal (propulsion) force proportional to the substrate thermal gradient and the viscous (drag) force proportional to the drop velocity. The drop velocity as a function of the thermal gradient is then readily obtained by setting the sum of these two forces equal to zero.

Overall, a complete parametric study has been carried out, predicting the shape asymmetries, drop velocities, and forces as functions of the drop size, superheat, thermal gradient, and fluid properties. In particular, for a given thermal gradient, larger drops are found to move faster and their shape asymmetries turn out to be greater.

As further perspectives, let us mention first of all a possible extension to more realistic, 3D Leidenfrost drops. As it is indicative from the present study, it may be more than sufficient to realize such an extension in the framework of just a linearized version of our approach. Another point concerns the quasi-steady approximation implied here throughout, including the treatment of the drop motion. In view of the drop inertia, however, a transient regime that would ensue upon the deposition of a Leidenfrost drop on a flat substrate with a thermal gradient seems to be quite worth of being studied. At last, we have here assumed a uniform thermal gradient. Physically, this means that it varies at the scales much larger than the drop size. However, it may well be of interest to consider in future studies the cases when it varies more abruptly, here possibly including what one could refer to as "thermal ratchets."

ACKNOWLEDGMENTS

The authors gratefully acknowledge the financial support of Fonds de la Recherche Scientifique—FNRS (FRFC–ODILE contract, Postdoctoral Researcher position of BS, Senior Research Associate position of SD, and Research Director position of PC), ESA-BELSPO (PRODEX projects), and BELSPO (IAP 7/38 μ-MAST project). This research was also carried out under COST Action MP1106's umbrella.

APPENDIX: VARIATION OF VAPOR PROPERTIES WITH THE TEMPERATURE

The physico-chemical properties of the vapor considered to depend on the temperature T are the density, ρ_v, the thermal conductivity, λ_v, and the dynamic viscosity, μ_v. As the vapor is treated as an ideal gas, ρ_v is expressed as follows:

$$\rho_v = \frac{PM}{R_g T}, \tag{A1}$$

where P, M, and R_g are the pressure, the molar mass, and the universal gas constant, respectively.

λ_v is computed using the semi-empirical equation developed by Eucken,[20]

$$\lambda_v = \mu_v \left(C_{p_v} + \frac{5}{4} \frac{R_g}{M} \right). \tag{A2}$$

The temperature dependence of the heat capacity C_{p_v} is weak and neglected here.

Finally, the dynamic viscosity is expressed using the Sutherland's equation,[21]

$$\mu_v = \mu_{v0} \left(\frac{T_0 + S}{T + S} \right) \left(\frac{T}{T_0} \right)^{3/2}, \tag{A3}$$

where μ_{v0} is the dynamic viscosity at the reference temperature T_0 and S is the Sutherland's constant.

For water, we used $M = 18.02$ g/mol, $C_{p_v} = 1410$ J/kg K, $S = 630$ K, and $\mu_{v0} = 10.0 \times 10^{-6}$ Pa s at $T_0 = 300$ K.

[1] J. G. Leidenfrost, *De Aquae Communis Nonnullis Qualitibus Tractatus, Part 2* (Hermannus Ovenius, Duisburg, 1756).
[2] H. Linke, B. Alemán, L. Melling, M. Taormina, M. Francis, C. Dow-Hygelund, V. Narayanan, R. Taylor, and A. Stout, "Self-propelled Leidenfrost droplets," Phys. Rev. Lett. **96**(15), 154502 (2006).
[3] G. Dupeux, M. Le Merrer, G. Lagubeau, C. Clanet, S. Hardt, and D. Quéré, "Viscous mechanism for Leidenfrost propulsion on a ratchet," Europhys. Lett. **96**, 58001 (2011).
[4] G. Lagubeau, M. Le Merrer, C. Clanet, and D. Quéré, "Leidenfrost on a ratchet," Nat. Phys. **7**(5), 395–398 (2011).
[5] G. Dupeux, M. Le Merrer, C. Clanet, and D. Quéré, "Trapping Leidenfrost drops with crenelations," Phys. Rev. Lett. **107**(11), 114503 (2011).
[6] A. Würger, "Leidenfrost gas ratchets driven by thermal creep," Phys. Rev. Lett. **107**(16), 164502 (2011).
[7] T. R. Cousins, R. E. Goldstein, J. W. Jaworski, and A. I. Pesci, "A ratchet trap for Leidenfrost drops," J. Fluid Mech. **696**, 215–227 (2012).
[8] Á. Marín, D. Arnaldo del Cerro, G. Romer, B. Pathiraj, A. Huis in't Veld, and D. Lohse, "Capillary droplets on Leidenfrost micro-ratchets," Phys. Fluids **24**, 122001 (2013).
[9] T. Baier, G. Dupeux, S. Herbert, S. Hardt, and D. Quéré, "Propulsion mechanisms for Leidenfrost solids on ratchets," Phys. Rev. E **87**, 021001 (2013).

[10]S. Hardt, S. Tiwari, and T. Baier, "Thermally driven flows between a Leidenfrost solid and a ratchet surface," Phys. Rev. E **87**, 063015 (2013).
[11]D. Soto, G. Lagubeau, C. Clanet, and D. Quéré, "Surfing on a herringbone," Phys. Rev. Fluids **1**, 013902 (2016).
[12]G. Dupeux, T. Baier, V. Bacot, S. Hardt, C. Clanet, and D. Quéré, "Self-propelling uneven Leidenfrost solids," Phys. Fluids **25**, 051704 (2013).
[13]J. Ok, E. Lopez-Ona, D. Nikitopoulos, H. Wong, and S. Park, "Propulsion of droplets on micro- and sub-micron ratchet surfaces in the Leidenfrost temperature regime," Microfluid. Nanofluid. **10**, 1045–1054 (2011).
[14]K. Piroird, C. Clanet, and D. Quéré, "Magnetic control of Leidenfrost drops," Phys. Rev. E **85**, 056311 (2012).
[15]B. Sobac, A. Rednikov, S. Dorbolo, and P. Colinet, "Leidenfrost effect: Accurate drop shape modeling and new scaling laws," Phys. Rev. E **90**, 053011 (2014).
[16]J. H. Snoeijer, P. Brunet, and J. Eggers, "Maximum size of drops levitated by an air cushion," Phys. Rev. E **79**, 036307 (2009).
[17]Y. Pomeau, M. Le Berre, F. Celestini, and T. Frisch, "The Leidenfrost effect: From quasi-spherical droplets to puddles," C. R. Méc. **340**, 867–881 (2012).
[18]J. C. Burton, A. L. Sharpe, R. C. A. van der Veen, A. Franco, and S. R. Nagel, "Geometry of the vapor layer under a Leidenfrost drop," Phys. Rev. Lett. **109**, 074301 (2012).
[19]A.-L. Biance, C. Clanet, and D. Quéré, "Leidenfrost drops," Phys. Fluids **15**(6), 1632–1637 (2003).
[20]A. Eucken, "Über das Wärmeleitvermögen, die spezifische Wärme und die innere Reibung der Gase," Physik. Zeits. **14**, 324–332 (1913).
[21]W. Sutherland, "The viscosity of gases and molecular force," Philos. Mag. Ser. **5**(36), 507–531 (1893).